AIAA JOURNAL
Vol. 39, No. 6, June 2001

Theoretical Model for Airfoils to Suppress Leading-Edge Separation

W. W. H. Yeung*
Nanyang Technological University, Singapore 639798, Republic of Singapore

A theoretical study is presented for an airfoil fitted with an upper-surface flap undergoing leading-edge stall. Instead of delaying or circumventing flow separation, flow is allowed to separate tangentially from an airfoil with a portion of its suction side truncated. The separation streamline is, thus, made to reattach smoothly at the tip of a streamlined forward-facing flap, which joins the airfoil tangentially to eschew any unnecessary stagnated flow. Different from conventional free-streamline models, the pressure along the bounding streamline is not assumed constant in the present model. Rather, finite velocities (whose values are unknown a priori) are achieved at separation, reattachment, and the trailing edge of the airfoil by utilizing mathematical singularities such as a vortex located inside the hollow airfoil. Furthermore, the condition of a finite pressure gradient at reattachment as deduced from available experimental data is proposed. The resulting lift is found to be larger than that of the basic Joukowsky airfoil for a wide range of angle of attack because the bounding streamline increases the airfoil camber. The modified profile may be considered as a new family of Joukowsky airfoil.

Nomenclature

A, B	=	mapping constants
c	=	chord
c_L	=	lift coefficient
c_p	=	pressure coefficient
f	=	mapping constant
G	=	complex function
h	=	length of flap
i	=	$\sqrt{-1}$
m, n	=	mapping constants
p, p_∞	=	pressure
Q_D	=	strength of doublet
R	=	radius of circle in Z_1 plane
R_V	=	radial distance of vortex
r^*	=	real constant
U, V	=	uniform upstream velocities
W	=	complex velocity
x, y	=	coordinates
Z, Z_1, $Z_{1,0}$, Z_2, Z_3, Z_4	=	complex numbers
$Z_{4,\infty}$, $\tilde{Z}_{4,\infty}$	=	complex numbers
α	=	angle of attack
α^*, β, δ, θ_0, θ, θ^*, σ	=	angles
Γ_1, Γ_2	=	vortex strengths
ε, μ	=	positive constants
ζ	=	complex plane
Λ	=	positive constant
ρ	=	density

Introduction

LEADING-EDGE stall, as investigated by McCullough and Gault,[1] is caused by abrupt flow separation near the leading edge, generally without subsequent reattachment. The associated flowfield is clearly revealed by the flow visualization by Werlé[2] at $\alpha = 15$ deg using air bubbles. This type of stall takes place on most airfoil profiles of moderate thickness, when the angle of attack for maximum lift is exceeded. The experimental pressure distributions reported by McCullough and Gault[1] on the stalled NACA 63-009 airfoil in Figs. 1b ($\alpha = 9$ deg) and 1c ($\alpha = 10$ deg) at a Reynolds number of 4.1×10^6 depict a region of more or less constant suction on the upper surface stemming from the leading edge. Apparently, they are in sharp contrast to a suction peak associated with the nonstalled situation in Fig. 1a ($\alpha = 8.9$ deg) at a Reynolds number of 5.8×10^6. Some characteristics have been identified as follows: 1) The region of nearly constant pressure occupies the first 10% chord of the airfoil at $\alpha = 9$ deg, and a considerable recovery of pressure is found downstream. 2) The chordwise extent of such a region lengthens with increasing angle of attack. 3) Reversed flow has been detected by surface tufts over a length of 20% chord measured from the leading edge. Beyond this point, although the flow is exceedingly rough, tufts always show flow in the downstream direction without the definite pattern of separated flow. 4) Detailed flow surveys near the leading edge of the NACA 63-009 airfoil reveal the presence of a circulation bubble, which is first discernible at $\alpha = 4$ deg and persists up to the stall. Because only a short extent of nearly constant surface pressure exists within the bubble, pressure recovery begins upstream of the point of flow reattachment. In general, when leading-edge stall occurs, there is a considerable loss of lift and increase in pressure drag.

Experimentally, mechanical devices such as leading-edge slats, as described by Abbott and von Doenhoff,[3] as well as Krüger flaps[4] have been used to delay leading-edge stall through increasing both maximum lift and the angle of attack for maximum lift. The application of a smooth or splined rotating cylinder embedded in the airfoil surface to prevent or delay separation, as extensively studied by Modi et al.,[5] has shown a significant delay in the stall angle and an increase in the lift coefficient at high angles of attack. The Kasper wing (see Ref. 6), which consists of leading-edge and trailing-edge split flaps to maintain an extensive region of vortex flow over the upper surface, has remarkable lift-to-drag ratios. Sucking air off of the vortex chambers on the downstream portion of the upper surface of a thick wing, as reported by Savitsky et al.,[7] has provided another means of boundary-layer control to overcome separation. These vortex chambers accommodate streamlined bodies and communicate with a low-pressure source through a common passage and a receiver. It has also been shown recently by Traub[8] that a vortex flap on a sharp-edged delta matches the performance, that is, in lift and drag, with a blunt-edge delta wing. Therefore, using vortices to delay stall and to enhance lift is a common practice.

An inviscid theory for leading-edge stall on an airfoil was developed by Cheng and Smith.[9] The vortex-induced lift on two-dimensional wings has been investigated theoretically by Saffman and Tanveer.[10] A variety of fence geometries and angles of attack on a Clark-Y airfoil have been studied by Rossow,[11] using an inviscid flow model to determine the characteristics of trapped-vortex, high-lift devices. More recently, the high-Reynolds-number asymptotics

Received 31 May 2000; revision received 27 September 2000; accepted for publication 18 October 2000.

*Associate Professor, School of Mechanical and Production Engineering.

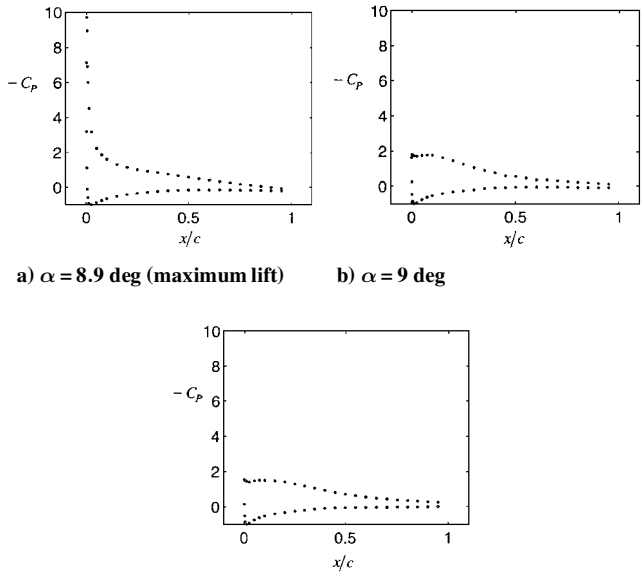

a) $\alpha = 8.9$ deg (maximum lift) b) $\alpha = 9$ deg

c) $\alpha = 10$ deg

Fig. 1 Experimental pressure distributions on NACA 63-009 from Ref. 1.

of a flow past an airfoil with a vortex trapped in a cavity was studied by Bunyakin et al.[12] for enhancing the airfoil performance.

In a previous study by Yeung and Parkinson,[13] the lift on a flat plate experiencing thin-airfoil stall has been shown theoretically to increase by as much as 20% when a forward-facing flap is added. Such lift enhancement is achieved by reattaching the separation streamline emanating from the leading edge to the tip of a forward-facing flap, which tangentially joins the upper surface of the plate. In the context of potential flow, this streamline acts like a solid boundary, adding positive camber to the flat plate.

Instead of modeling leading-edge stall, a theoretical study for Joukowsky airfoils of arbitrary thickness and camber is presented here to demonstrate how the leading-edge separation streamline and a forward-facing flap located on the upper surface can increase the airfoil camber and lift. Considerable progress has been made with respect to the flat plate case[13] in terms of constructing a new mapping sequence to create a hollow airfoil for smooth separation near the leading edge. Such a smooth separation is vital in the theoretical model to produce realistic pressure distributions. The conditions of tangential reattachment at the flap tip and smooth separation at the trailing edge are also satisfied. It has been successfully demonstrated that the three-vortex model (with the doublet model as its limiting case) used for the flat plate is also applicable to the airfoil.

By the use of the hodograph method, Hurley[14] proposed a similar concept in which a very thick pseudowing is made up of a free streamline joining the leading edges of two flat plates of unequal lengths hinged at the trailing edge. The present model is different from Hurley's airfoil in the following respects:

1) The rigid boundary of Hurley's[14] airfoil is made up of straight lines, whereas that of the present model consists of an airfoil, which is truncated on its upper surface, and a forward-facing flap, all streamlined.

2) The hodograph method used by Hurley[14] requires the velocity (or pressure) along the free streamline to be constant. The separation streamline in the current study is a non-conventional one, and such a requirement is, therefore, unnecessary.

3) The complex velocity in Hurley's[14] airfoil consists of a uniform flow, a doublet, and a vortex, but additional flow elements are required in the current model to create a bounding streamline joining the leading edge of the airfoil and the flap tip.

4) As clearly indicated by McCullough and Gault,[1] relatively constant pressure exists over a short extent of the separation bubble, and the pressure begins to recover when approaching reattachment, which is expected to be downstream of such a suction plateau. Note from Figs. 1b and 1c that the pressure gradient in such a region is gradual. As a result, the condition of a finite pressure gradient at reattachment on the flap tip is proposed in the present study. Such a condition was not explored in Hurley's[14] model.

5) In the experimental study, Hurley[14] proposed the use of blowing high-speed air from a slot located near the leading edge of the upper boundary to achieve flow reattachment. Such a usage of external source of flow was never incorporated in Hurley's theoretical model. In the present theory, a vortex located inside the truncated airfoil has been explicitly identified to achieve flow reattachment. In other words, no additional net flow is needed, and any means enabling the flow to be circulated inside the truncated airfoil may be used to realize it physically.

In subsequent sections, details of constructing the airfoil and the forward-facing flap are presented. Both the flap shape and the flap length are independent of the angle of attack, but the deformable streamline is determined by the solution at one α. The effects of varying the location of separation, flap length, and flap location and the original airfoil camber are studied with the help of the three-vortex model. Note that the doublet model, which was presented in Ref. 13, is a limiting case where the condition of the finite pressure gradient at reattachment is not satisfied. Comparisons are made with the classical theory of Joukowsky (see Ref. 3) in terms of pressure and lift to demonstrate that lift is augmented.

Theory

Mapping Sequence

The Joukowsky airfoil of arbitrary camber and thickness is used here as the prototype airfoil for leading-edge stall. The mapping sequence is shown in Fig. 2, where portion LB on its upper surface in the physical plane Z (Fig. 2a) is truncated such that flow separates tangentially at L. Under a standard Joukowsky transformation,

$$Z = A(Z_1 + 1/Z_1) + B \tag{1}$$

where $A = 1/(2+\Lambda)$, $B = \Lambda/(2+\Lambda)$, and $\Lambda = 1 + 2\varepsilon + 1/(1+2\varepsilon)$. The incomplete airfoil becomes a circular-arc slit (Fig. 2b) in the Z_1 plane. This slit passes through $Z_1 = 1$, that is, point T, and is centered at $Z_{1,0} = -\varepsilon + i\mu$, of which the real and imaginary parts determine the camber and thickness of the airfoil, respectively. The chordwise location of point L is x_L/c, obtained by taking the real part of Eq. (1) with $Z_1 = Z_{1,0} + R\exp(i\sigma)$, where $R = |1 - Z_{1,0}|$ is

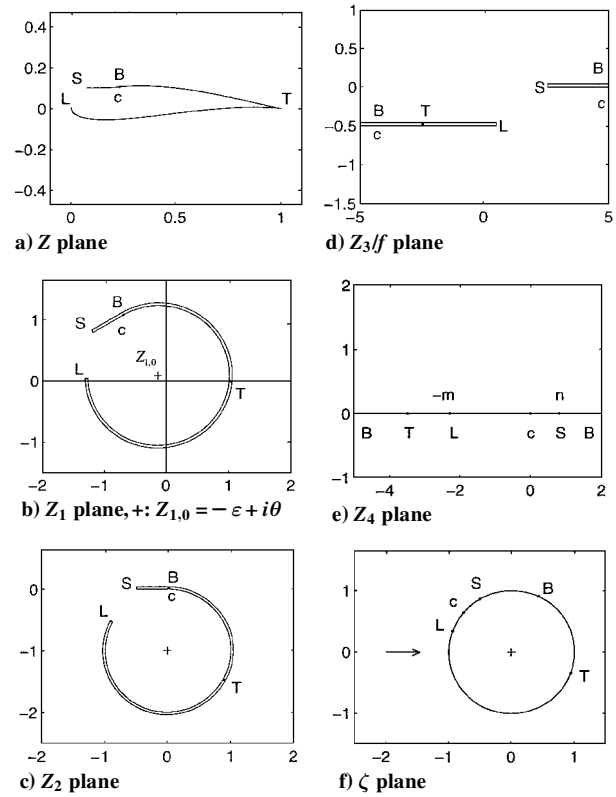

a) Z plane d) Z_3/f plane

b) Z_1 plane, +: $Z_{1,0} = -\varepsilon + i\theta$ e) Z_4 plane

c) Z_2 plane f) ζ plane

Fig. 2 Mapping sequence.

the radius of the circular arc. A straight-line segment SB in both the Z_1 and Z_2 planes becomes a forward-facing flap in the Z plane. It lies along the negative real axis in the Z_2 plane (Fig. 2c) and has a length equal to h. Point S is where the separation streamline from point L joins the flap. The mapping between the Z_1 and Z_2 planes is

$$Z_2 = -i + (Z_1 - Z_{1,0})R^{-1}\exp(-i\theta_0) \tag{2}$$

which consists of a rotation about $Z_{1,0}$ through an angle θ_0 in the Z_1 plane, a scaling and a translation of point B to the origin of the Z_2 plane. Thus, the center of the circular-arc slit of unit radius in the Z_2 plane is at $Z_2 = -i$. Note that the chordwise location of the flap base x_B/c, which is equal to the real part of Eq. (1) with $Z_1 = Z_{1,0} + R\exp(i\theta_0)$, specifies the value of θ_0. Under the product mapping,

$$Z_2 Z_3 = -f \tag{3}$$

the continuous contour LBS in the Z_2 plane is split at point B to form two semi-infinite horizontal lines in the Z_3/f plane (Fig. 2d), where $\mathrm{Im}(Z_3/f) = -\frac{1}{2}$ for LB and $\mathrm{Im}(Z_3) = 0$ for BS. Note that the point of infinity $Z = \infty$ is mapped to $Z_3 = 0$. The Schwartz–Christoffel transformation

$$Z_3 = Z_4 + mn/Z_4 + (m-n)\log Z_4 \tag{4}$$

rejoins LB and SB to form the real axis of the Z_4 plane with point S at $Z_4 = n(>0)$, point L at $Z_4 = -m(<0)$, and point B at $Z_4 = \pm\infty$ (Fig. 2e). A unit circle $\zeta = \exp(i\theta)$ (Fig. 2f) is mapped from the Z_4 plane by the bilinear transformation

$$\zeta = \frac{-\tilde{Z}_{4,\infty} + Z_4}{Z_{4,\infty} - Z_4}\exp(i\alpha^*) \tag{5}$$

where complex constant $Z_{4,\infty}$ is the image of the point of infinity, and $\tilde{Z}_{4,\infty}$ is the complex conjugate of $Z_{4,\infty}$. For given values of h, θ_0, and σ, Eqs. (3) and (4) are combined to give the following nonlinear equations for determining the values of f, m, and n:

$$f/h = m + n + (m-n)\log n \tag{6}$$

$$-f/2 = (m-n)\pi \tag{7}$$

$$(f/2)\cot[(\sigma-\theta_0)/2] = -(m+n) + (m-n)\log m \tag{8}$$

For a physically admissible situation, it is required that $\sigma > \theta_0$. If $Z_{4,\infty} = r^*\exp(i\theta^*)$, which corresponds to the image of $Z_3 = 0$ in the Z_4 plane, then r^* and θ^* can be found from equating the real and imaginary parts of Eq. (4) to give

$$0 = (r^* + mn/r^*)\cos\theta^* + (m-n)\log r^* \tag{9}$$

$$0 = (r^* - mn/r^*)\sin\theta^* + (m-n)\theta^* \tag{10}$$

provided the values of m and n are known from solving Eqs. (6–8). Variations of (f, m, n) and (r^*, θ^*) in Fig. 3 correspond to indicated values of $Z_{1,0}$, x_L, x_B, and h.

The complex velocity $W(Z)$ in the physical plane can be related to the complex velocity $W(\zeta)$ in the ζ plane by

$$W(Z) = \frac{W(\zeta)}{\mathrm{d}Z/\mathrm{d}\zeta} \tag{11}$$

If the flow far away from the airfoil in Fig. 2a is represented by $U\exp(-i\alpha)$ and that from the unit circle in Fig. 2f is V, that is, zero inclination, then

$$\frac{V}{U} = \left|\frac{\mathrm{d}Z}{\mathrm{d}\zeta}\right|_\infty \tag{12}$$

$$\alpha^* = \theta_0 + \pi - (\alpha + \beta) \tag{13}$$

where $\beta = \arg[1 - mn/Z_{4,\infty}^2 + (m-n)/Z_{4,\infty}^2]$. As a result, α^* in Eq. (5) is determined by Eq. (13). The pressure distributions on the airfoil, bounding streamline, and flap can be determined by Bernoulli's equation:

$$c_p = 2(p - P_\infty)\big/ pU^2 = 1 - |w(Z)/U|^2 \tag{14}$$

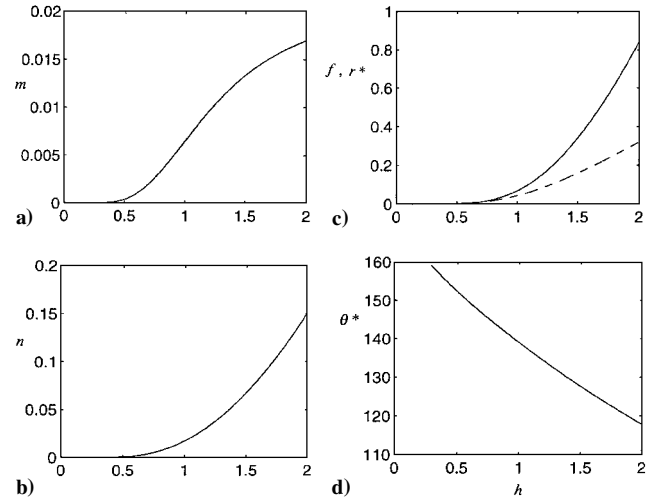

Fig. 3 Variations of a) m, b) n, c) f (——) and r^* (– – –), and d) θ^* with h for $Z_{1,0} = (-0.14, 0)$ and $(x_L, x_B)/c = (0, 0.5)$.

The critical points of the mapping sequence, which can be found by equating the derivative

$$\frac{\mathrm{d}Z}{\mathrm{d}\zeta} = \frac{-iAR\exp(i\theta_0 - i\alpha^*)}{-\tilde{Z}_{4,\infty} + Z_{4,\infty}}\left(1 - \frac{1}{Z_1^2}\right)\frac{f}{Z_3^2} \times\left(1 - \frac{mn}{Z_4^2} + \frac{m-n}{Z_4}\right)(Z_{4,\infty} - Z_4)^2 \tag{15}$$

to zero are at $Z_1 = 1$ for the trailing edge (point T) of the airfoil, $Z_4 = -m$ for the separation point (point L), and $Z_4 = n$ for the tip of the forward-facing flap (point S). It can be shown readily by applying l'Hôpital's rule to $(Z_{4,\infty} - Z_4)/Z_3$ that $\mathrm{d}Z/\mathrm{d}\zeta$ is nonzero at the base of the flap, that is, $Z_3 = \infty$, and at another point where $Z_4 = Z_{4,\infty}$. To achieve finite velocity at the critical points, Eq. (11) requires that

$$W(\zeta) = 0 \qquad \text{at } \zeta = \exp(i\theta_L), \exp(i\theta_T), \exp(i\theta_S) \tag{16}$$

That is, the critical points coincide with the stagnation points in the ζ plane. The pressure coefficient at each of the critical points is calculated by

$$c_p = 1 - \left|\frac{1}{U}\frac{\mathrm{d}W(\zeta)/\mathrm{d}\zeta}{\mathrm{d}^2Z/\mathrm{d}\zeta^2}\right|^2 \tag{17}$$

because these critical points are simple zeros of $\mathrm{d}Z/\mathrm{d}\zeta$. When Eq. (15) is differentiated, it can be shown that

$$\left|\frac{\mathrm{d}^2Z}{\mathrm{d}\zeta^2}\right|_T = 2A\left|\frac{Rf}{Z_3^2}\left(1 - \frac{mn}{Z_4^2} + \frac{m-n}{Z_4}\right)\frac{(Z_{4,\infty} - Z_4)^2}{(-\tilde{Z}_{4,\infty} + Z_{4,\infty})}\right|_T^2 \tag{18}$$

$$\left|\frac{\mathrm{d}^2Z}{\mathrm{d}\zeta^2}\right|_L = ARf\left(\frac{m+n}{m^2}\right)\left|\left(1 - \frac{1}{Z_1^2}\right)\frac{1}{Z_3^2}\frac{(Z_{4,\infty} + m)^4}{(-\tilde{Z}_{4,\infty} + Z_{4,\infty})^2}\right|_L \tag{19}$$

$$\left|\frac{\mathrm{d}^2Z}{\mathrm{d}\zeta^2}\right|_S = ARf\left(\frac{m+n}{n^2}\right)\left|\left(1 - \frac{1}{Z_1^2}\right)\frac{1}{Z_3^2}\frac{(Z_{4,\infty} - n)^4}{(-\tilde{Z}_{4,\infty} + Z_{4,\infty})^2}\right|_S \tag{20}$$

Flow Model

The circumference of the unit circle centered at the origin of the ζ plane is mapped from the contours of the hollow airfoil and the forward-facing flap. To simulate the flow around the circle, a combination of uniform flow V, doublet of strength V situated at $\zeta = 0$, and vortex of strength Γ_1 located at the origin is used. Therefore, the complex velocity for such basic flow elements is given by

$$W_B(\zeta) = V(1 - 1/\zeta^2) + i\Gamma_1/2\pi\zeta \tag{21}$$

where Γ_1 is an unknown. Additional flow elements, which are subject to the boundary conditions imposed by the critical points, are required to create a streamline emanating from the separation point L and reattaching to the tip of the flap at point S. In other words, the net flow produced by these elements over a closed contour surrounding them is zero. The three-vortex model proposed in Ref. 13 fulfills such a requirement. It consists of placing a vortex of strength Γ_2 at $\zeta = R_V \exp(i\delta)$, where $R_V > 1$, external to the unit circle. According to the circle theorem by Milne-Thomson,[15] an image at $\zeta = \exp(i\delta)/R_V$ and another at $\zeta = 0$ are required for the circle to remain as a streamline. By combining the image at the origin with the vortex in W_B,

$$W(\zeta) = W_B(\zeta) + (i\Gamma_2/2\pi)(1/\{\zeta - R_V \exp[i\delta]\} - 1/\{\zeta - \exp[i\delta]/R_V\}) \tag{22}$$

In the limit that $R_V \to 1$, it can be shown that

$$\frac{i\Gamma_2}{2\pi}\left\{\frac{1}{\zeta - R_V \exp[i\delta]} - \frac{1}{\zeta - \exp[i\delta]/R_V}\right\} \to \frac{i\Gamma_2(R_V - 1/R_V)\exp(i\delta)}{2\pi(\zeta - \exp[i\delta])^2} \tag{23}$$

indicating that the three-vortex model is equivalent to the doublet model[13] with $\Gamma_2(R_V - 1/R_V)$ being the strength of a doublet tangential to the unit circle $\zeta = \exp(i\theta)$ at the angular location δ. Although the doublet model is the simplest model because the three unknowns can be uniquely determined by the conditions imposed by the critical points, it produces a rather nonsmooth pressure gradient at reattachment. Another possible choice is a combination of a source and a sink of the same strength because it also produces zero net flow. However, detailed calculations have shown that the additional lift associated with this model is not as large as that from the following three-vortex model, and so it is not discussed further here.

A condition additional to $W(\zeta) = 0$ at L, S, and T is required to determine Γ_1, Γ_2, R_V, and δ. As elaborated in the introduction and also in Ref. 13, a possible choice is to impose the condition of a finite pressure gradient at flow reattachment or the flap tip. This condition also implies that the streamline at reattachment also possesses finite curvature. The corresponding expression is

$$\left|\frac{dW(\zeta)}{d\zeta}\right|\left|\frac{d^3Z}{d\zeta^3}\right| - \left|\frac{d^2W(\zeta)}{d\zeta^2}\right|\left|\frac{d^2Z}{d\zeta^2}\right| = 0 \tag{24}$$

where each term in Eq. (24) is evaluated at $\zeta = \exp(i\theta_S)$. Both $dW(\zeta)/d\zeta$ and $d^2W(\zeta)/d\zeta^2$ can be obtained by straightforward differentiation of Eqs. (21) and (22). Whereas Eq. (20) provides the expression for $d^2Z/d\zeta^2$ at point S, the derivation of $d^3Z/d\zeta^3$ from Eq. (15) is routine but lengthy. The result is simplified to

$$\frac{d^3Z}{d\zeta^3} = \frac{-iARf\exp\left[i\left(\theta_0 - \alpha^*\right)\right]}{(-\tilde{Z}_{4,\infty} + Z_{4,\infty})}G \tag{25}$$

where

$$G = \left(1 - \frac{1}{Z_1^2}\right)\frac{1}{Z_3^2}\left[\frac{-6mn}{Z_4^4} + \frac{2(m-n)}{Z_4^3}\right] \times \frac{(Z_{4,\infty - Z_4})^6 \exp(-2i\alpha^*)}{(-\tilde{Z}_{4,\infty} + Z_{4,\infty})^2} + \left(1 - \frac{1}{Z_1^2}\right)\frac{1}{Z_3^2} \times \left(\frac{2mn}{Z_4^3} - \frac{m-n}{Z_4^2}\right)\frac{(-6)(Z_{4,\infty - Z_4})^5 \exp(-2i\alpha^*)}{(-\tilde{Z}_{4,\infty} + Z_{4,\infty})^2}$$

The lift coefficient resulting from the three-vortex model can be calculated either by integrating the chordwise c_p distribution from Eqs. (14) and (17) or by determining the value of Γ_1 from solving Eqs. (16) and (24).

Results and Discussion

As reported in Ref. 5, a symmetrical 16% thick basic Joukowsky airfoil attains its maximum lift at $\alpha = 16$ deg and experiences leading-edge stall at $\alpha = 18$ deg when tested in a wind tunnel at a Reynolds number of 2.31×10^5. As a result, such angles of attack are used as a reference here. The classical theory of Joukowsky (see Ref. 3) for attached flow is included to show the modification of airfoil profile and to assess if the present model provides realistic pressure distributions and lift variations.

Figures 4a–4d depict the shape of the separation streamline and the location of the external vortex in the Z_1, Z_2, Z_3, and Z_4 planes for the three-vortex model at $\alpha = 18$ deg, $h = 0.55$, $Z_{10} = (-0.14, 0)$, and $(x_L, x_B)/c = (0, 0.5)$. In the physical plane Z (Fig. 5a), the new airfoil is compared with the original profile. It is found that the external vortex is slightly lower than the slit LB in the Z_3 plane in Fig. 4c and also lies slightly under the truncated portion of the airfoil in the Z plane. The locations of external vortex and its two

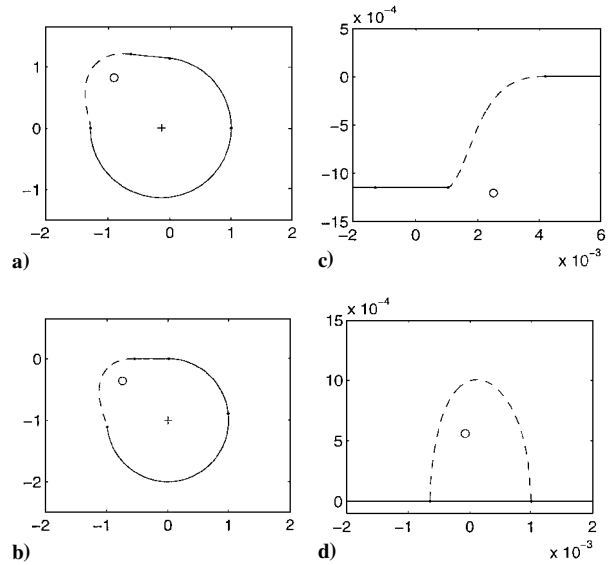

Fig. 4 Shapes of bounding streamline (– – –) and locations (○) of external vortes in a) Z_1, b) Z_2, c) Z_3, and d) Z_4 plane for $\alpha = 18$ deg, $h = 0.55$, $Z_{1,0} = (-0.14, 0)$, and $(x_L, x_B)/c = (0, 0.5)$.

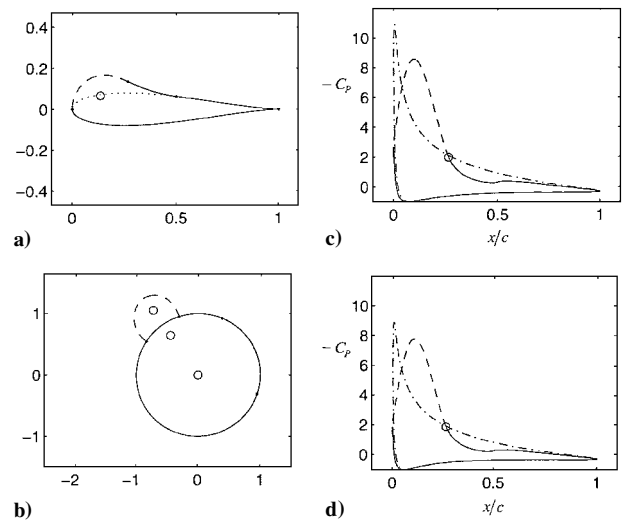

Fig. 5 Shapes of bounding streamline (– – –) and locations (○) of vortices in a) Z plane and b) ζ plane; comparison of pressure distributions (– ·–, basic profile) and (——, – – –, present profile) at c) $\alpha = 18$ deg (leading-edge stall) and d) $\alpha = 16$ deg (maximum lift).

Table 1 Results of present model and Joukowsky profile

	$\alpha = 18$ deg		$\alpha = 16$ deg	
Parameter	Original profile	Present	Original profile	Present
$\min(c_p)$	−10.89	−8.56	−8.88	−7.77
x/c at $\min(c_p)$	0.003	0.097	0.004	0.1040
$\max(y/c)$	0.0795	0.1670	0.0795	0.1664
x/c at $\max(y/c)$	0.2563	0.1560	0.2563	0.1565
c_L	2.18	2.43	1.95	2.18
c_p at $x/c = 0$	−9.06	−1.98	−7.01	−1.39

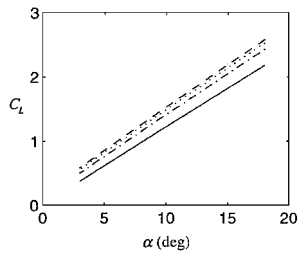

a) – ·–, $h = 0.55$; · · ·, $h = 0.75$; and – – –, $h = 0.85$

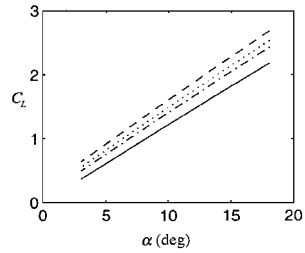

b) – ·–, $x_B/c = 0.5$; · · ·, $x_B/c = 0.6$; and – – –, $x_B/c = 0.7$

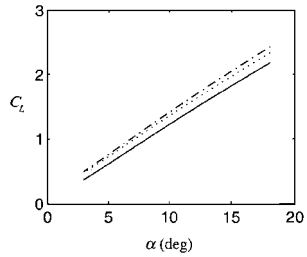

c) – ·–, $x_L/c = 0$ and · · ·, $x_L/c = 0.05$

Fig. 6 Lift cofficient vs angle of attack (——, basic profile).

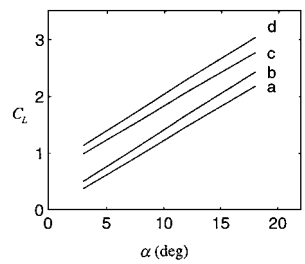

Fig. 7 Lift coefficient vs angle attack with $(x_L, x_B)/c = (0, 0.5)$: a) basic Joukowsky, b) three-vortex model with $h = 0.55$ and $Z_{1,0} = (-0.14, 0)$, c) basic Joukowsky, and d) three-vortex model with $h = 0.55$ and $Z_{1,0} = (-0.14, 0.1)$.

images in the ζ plane are shown in Fig. 5b. Note that the separation streamline reattaches tangentially at the flap tip in the Z_1, Z_2, Z_3, and Z planes, whereas the flap tip is a stagnation point in the Z_4 and ζ planes. Theoretical pressure distributions of the basic Joukowsky and the present model are compared in Fig. 5c at $\alpha = 18$ deg. Over the upper surface of the airfoil, the steep and narrow suction peak near the leading edge of the original profile is replaced by a gradual and broader suction peak of the modified profile, but shifted downstream of the leading edge. The pressure distributions on the lower surface are, however, almost identical. The pressure distributions at $\alpha = 16$ deg are shown in Fig. 5d. The finite pressure gradient at the flap tip is highlighted in both Fig. 5c and 5d. The effects of varying h, x_L, and x_B on the lift curve are depicted in Figs. 6a–6c. Table 1 summarizes some results of the present model and basic Joukowsky profile.

The effect of camber on the variation of lift with respect to the angle of attack can be examined by setting the imaginary part of $Z_{1,0}$ to be nonzero. Taking $h = 0.55$ and $(x_L, X_B)/c = (0, 0.5)$, curve d in Fig. 7 represents the lift variation from the three-vortex model when $Z_{1,0} = (-0.14, 0.1)$, whereas curve b corresponds to $Z_{1,0} = (-0.14, 0)$. Such variations for the basic Joukowsky profiles represented by curves c and a are included for comparison, indicating that the four curves are approximately parallel. From Fig. 7 and the following data, it is obvious that the three-vortex model provides larger lift and steeper lift curve slopes as compared with the basic profiles: For $\partial c_L/\partial\alpha$ (per degree), the basic symmetrical profile is 0.1207, the basic cambered profile is 0.1188, the present symmetrical profile is 0.1287, and the present cambered profile is 0.1269.

Conclusions

A theoretical investigation in reattaching the leading-edge separation streamline to the tip of an upper-surface flap of an airfoil is presented. It is found that truncating a portion of the airfoil and inserting a forward-facing flap on the downstream portion of the airfoil may allow a bounding streamline to form without creating unnecessary stagnation points at separation and reattachment. Realistic pressure distributions have been obtained when a flow model consisting of vortex located under the bounding streamline is used and the condition of finite pressure gradient is satisfied at the tip of the flap. The resulting streamline lies above the original basic profile such that the airfoil camber is increased. Generally, c_L increases with increasing flap length and the location of reattachment when the bounding streamline lengthens, but it decreases with increasing x_L (i.e., location of separation measured from leading edge) when the streamline shortens. The effect of camber on the lift and lift curve slope has also been examined. In general, the profile resulting from the three-vortex model may be treated as a new family of Joukowsky airfoils.

References

[1]McCullough, G. B., and Gault, D. E., "Examples of Three Representative Types of Airfoil-Section Stall at Low Speed," NACA TN 2502, 1951.

[2]Werlé, H., "Hydrodynamic Flow Visualization," *Annual Review of Fluid Mechanics*, Vol. 5, 1973, pp. 361–382.

[3]Abbott, I. H., and von Doenhoff, A. E., *Theory of Wing Sections*, Dover, New York, 1949, pp. 50–53.

[4]Krüger, W., "Wind Tunnel Investigation on a Changed Mustang Profile with Nose Flap. Force and Pressure Distribution Measurements," NACA TM 1177, 1947.

[5]Modi, V. J., Munshi, S. R., and Bandyopadhyay, G., "High-Performance Airfoil with Moving Surface Boundary-Layer Control," *Journal of Aircraft*, Vol. 35, No. 4, 1998, pp. 544–553.

[6]Cox, J., "The Revolutionary Kasper Wing," *Soaring*, Vol. 37, Dec. 1973, pp. 20–23; also U.S. Patent 3831885, Aug. 1974.

[7]Savitsky, A. L., Schukin, L. N., Karelin, V. G., Mass, A. M., Pushkin, R. M., Shibanov, A. P., Schukin, I. L., and Fischenko, S. V., "Method for Control of the Boundary Layer on the Aerodynamic Surface of an Aircraft, and the Aircraft Provided with the Boundary Layer Control System," U.S. Patent 5417391, 23 May 1995.

[8]Traub, L. W., "Comparative Study of Delta Wings with Blunt Leading Edges and Vortex Flaps," *Journal of Aircraft*, Vol. 33, No. 4, 1996, pp. 828–830.

[9]Cheng, H. K., and Smith, F. T., "The Influence of Airfoil Thickness and Reynolds Number on Separation," *Journal of Applied Mathematics and Physics (ZAMP)*, Vol. 33, 1982, pp. 151–180.

[10]Saffman, P. G., and Tanveer, S., "Vortex Induced Lift on Two Dimensional Low Speed Wings," *Studies in Applied Mathematics*, Vol. 71, No. 1, 1984, pp. 65–78.

[11]Rossow, V. J., "Aerodynamics of Airfoils with Vortex Trapped by Two Spanwise Fences," *Journal of Aircraft*, Vol. 31, No. 1, 1994, pp. 146–153.

[12]Bunyakin, A. V., Chernyshenko, S. I., and Stepanov, G. Yu., "High-Reynolds-Number Batchelor-Model Asymptotics of a Flow Past an Aerofoil with a Vortex Trapped in a Cavity," *Journal of Fluid Mechanics*, Vol. 358, 1998, pp. 283–297.

[13]Yeung, W. W. H., and Parkinson, G. V., "A Theoretical Investigation of Enhanced Lift in the Presence of Thin-Airfoil Stall," *Aeronautical Journal*, Vol. 103, No. 1023, 1999, pp. 237–244.

[14]Hurley, D. G., "The Use of Boundary Layer Control to Establish Free Streamline Flows," *Boundary Layer and Flow Control*, Vol. 1, edited by G. V. Lachmann, Pergamon, Oxford, 1964, pp. 265–294.

[15]Milne-Thomson, L. M., *Theoretical Aerodynamics*, Dover, New York, 1958, pp. 84, 85.

A. Plotkin
Associate Editor